Materials Research Proceedings 28 (2023) 149-158 https://doi.org/10.21741/9781644902479-17

Application of the plane-strain-compression-test to determine the local mechanical properties of LPBF-manufactured 316l components

JENSCH Felix[1,a *], BUHL Johannes[1,b], LAUE Robert[2,c] and HÄRTEL Sebastian[1,d]

[1]Chair of Hybrid Manufacturing (FHF), Brandenburg University of Technology, 03046 Cottbus, Germany

[2]Professorship Virtual Production Engineering, Chemnitz University of Technology, 09126 Chemnitz, Germany

[a]felix.jensch@b-tu.de, [b]johannes.buhl@b-tu.de, [c]robert.laue@mb.tu-chemnitz.de, [d]haertel@b-tu.de

Keywords: LPBF-Process, Local Properties, Plane-Strain-Compression-Test

Abstract. In the Laser Powder Bed Fusion (LPBF) process for metal components, a CAD file is sliced into layers with a thickness of 20-80 micrometers and the component is built up layer by layer. For this purpose, a metal powder layer is applied in each case and melted locally. This process is repeated until the geometry is completely established. The mechanical properties of the manufactured part are controlled by the cooling rate. It is currently not considered in the design of LPBF components, that the printed part has a varying heat flow into the surrounding powder and into the support plate depending on its slenderness. As a result of the different temperature histories, different microstructures with correspondingly different mechanical properties are formed in the untreated state (as-built). These differences must be considered in the component design. In this work, walls of various thicknesses were produced from 316L stainless-steel alloy using the LPBF process. The walls could be used to create plane-strain-compression-test specimens of various heights and orientations. The tests were performed according to Graf et al. [1] and the flow curve was calculated from the force-displacement curve while taking friction into account. Following that, tensile strength, Young's modulus, yield strength, and yield stress were determined inversely. A clear dependence of the mechanical parameters on the degree of slimness was discovered, which was confirmed by microscopic examinations. To summarize, the plane-strain-compression-test is a quick and reliable method for determining the local variation of mechanical properties.

Introduction

Since its development in the 1980s, additive manufacturing has gained in importance from year to year [2]. This results from the large variety of shapes that layer-by-layer construction makes possible. Thus, it is possible to manufacture topology-optimized components where material is only provided along the load paths [3]. Consequently, fewer resources are consumed for such components and the degree of lightweight design is maximized [4]. However, the optimized structure is often very complex and can only be manufactured with a great deal of effort or not at all using conventional manufacturing processes, such as milling or turning [5]. Additive manufacturing processes such as selective laser melting (SLM) are increasingly being used to produce complex shape-optimized geometries [6].

In most cases, the topology-optimized geometry consists of thin structures that converge at the connection points and thus lead to material accumulations. Since thicker component areas cool more slowly than narrow ones, different cooling rates develop in the different component areas [7]. In addition to the grain size, the cooling rate of the material determines the composition of the

microstructure. For example, in steels, martensitic, bainitic, ferritic, pearlitic and austenitic structures can develop [8]. In narrow areas, the cooling rate is higher, which is why a predominantly fine-grained martensitic or bainitic microstructure with an increased tensile strength develops [9]. In thicker areas, the cooling rate is lower, especially in the center of the cross-section, resulting in a coarser-grained softer ferritic or pearlitic microstructure with a lower tensile strength [10]. Furthermore, with an increased cooling rate, the average grain size decreases, which leads to strengthening by grain refinement [11]. Thus, depending on the cross-sectional area, a locally varying property profile develops over the component [12].

For complex components, empirical determination of the phase fractions and the resulting properties is only possible with a great deal of effort. Therefore, these are calculated by means of simulations. Zhang et al. determined the phase composition for Ti-6Al-4V by implementing a phenomenological phase transformation model into conventional simulation methods for additive manufacturing [13]. Another phenomenological microstructure model to determine the phase composition for Ti-6Al-4V was proposed by Nitzler et al. [14]. However, simulations of the L-PBF process to determine the phase composition take a lot of time and have no direct impact on the optimization of the part geometry.

In order to consider the properties resulting from the LPBF process during topology optimization, it is necessary to consider them in advance. This results in new challenges in the modeling of the anisotropic material behavior, the development of robust optimization algorithms and the integration of the process simulation into the structural optimization [15]. Considering the self-weight of the intermediate structure, the process-dependent loads, and the material properties dependent on the process time, Wang et al. provide an approach for a corresponding topology optimization [16]. Another possibility to consider process-dependent material properties is the description of geometry-dependent local material properties. A first step for this is the determination of the phase composition and its coupling with the mechanical properties depending on the slenderness of the manufactured structure.

The plane-strain-compression-test is an efficient test method for calculating the flow curve up to large plastic strains. It is based on the theoretical principles of the work of Nádai [17] and Orowan [18] and converted into a practical test for determining mechanical properties by Watts et al. [19] and Sellars et al. [20]. In this experiment, two opposing punches locally compress a strip-shaped sheet specimen. To avoid stress concentrations and consequently an early specimen failure due to fracture, the use of punches with rounded edges is recommended [21]. However, this increases the friction component, which must be eliminated by calculation to improve the quality of the results. In addition to friction, shearing, i.e. the deformation of material volume to the side of the punch, also has an influence on the measured force [22]. The ratio of punch width to specimen height influences both the friction component and the shear component. The larger this ratio is, the larger the friction component becomes and the smaller the shear component becomes [23]. The aim of the work is to efficiently obtain local flow stress differences in additively manufactured components using the plane-strain-compression-test, which is first investigated on small LPBF manufactured cuboids.

Materials and Methods

Specimen manufacturing.

The plane-strain-compression-specimens of 316L powder from m4p material solutions GmbH were produced with an EOS M290 from EOS GmbH. A laser power of approx. 200 W, a scanning speed of approx. 900 mm/s, a vector distance of 0.1 mm and a layer thickness of 0.04 mm were used. The laser was focused to a diameter of about 0.08 mm and the LPBF-process took place under argon atmosphere. Three narrow walls with a cross-section of 30 mm x 13 mm and a thickness of 1 mm, 1.5 mm, 2 mm and 3 mm were produced in each case in upright (0°) and horizontal (90°) orientation. These already have the final dimensions of the plane-strain-

compression-specimens and are used under as-printed conditions. Furthermore, three blocks each with the dimensions 30 mm x 13 mm x 25 mm were printed in upright and horizontal position. A plane-strain-compression-specimen with a thickness of 1 mm, 1.5 mm, 2 mm and 3 mm was eroded from each of these blocks by the wire EDM machine MAKINO U6 from Makino GmbH. (Fig. 1).

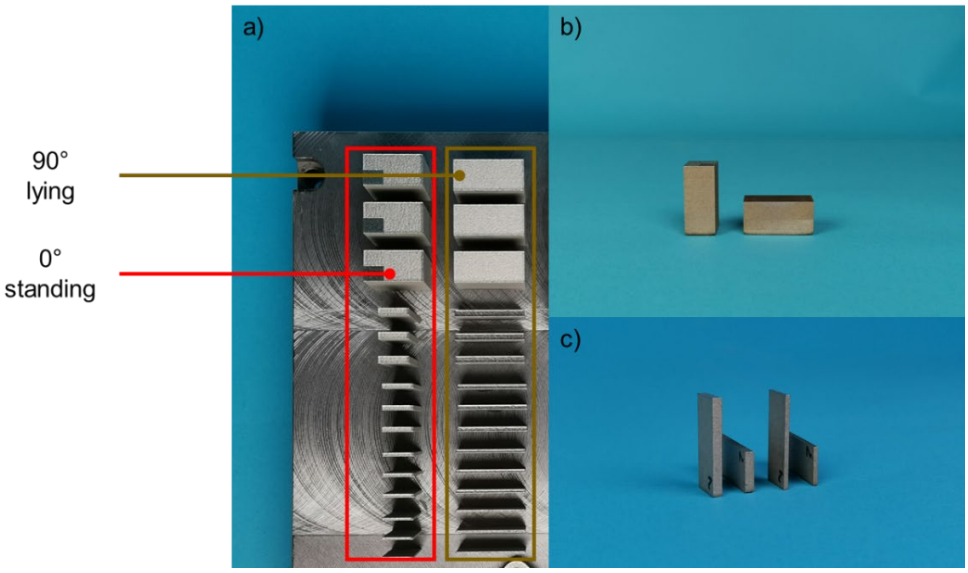

Fig. 1. Printed parts for the plane-strain-compression-test a) on the build plate, b) as blocks for wire EDM and c) as walls.

Plane-strain-compression-test.

The produced specimens were tested in a compression test on a Galdabini Quasar 50 universal testing machine with a maximum test load of 50 kN using 2.7 mm wide punches (Fig. 2). The tests took place under room temperature and with a quasi-static strain rate of $\dot{\varphi} = 0.01\ s^{-1}$ to avoid influences due to microstructural changes of the material.

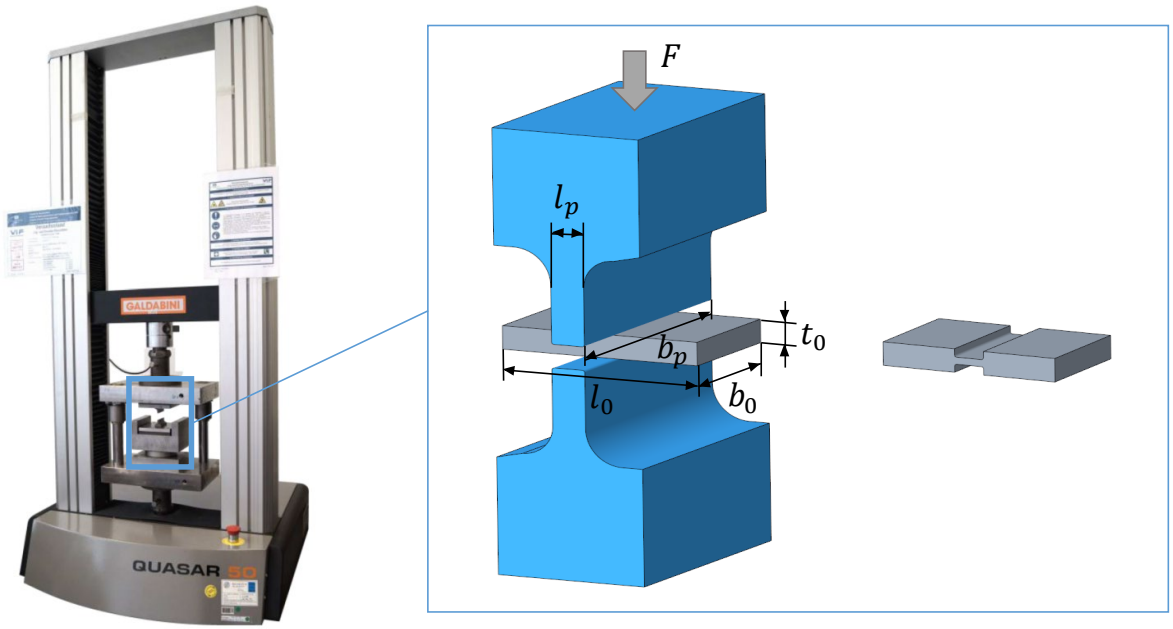

Fig. 2: Universal testing machine GALDABINI QUASAR 50 kN and the schematic structure of the plane-strain-compression-test.

During the test, raw data for applied force F and the distance Δt traveled by the punch. To determine the flow curve, the stress σ_{k_f} was calculated according to equation 1 and the corrected equivalent plastic strain φ according to equation 2 [24, 25].

$$\sigma_{k_f} = \frac{\sqrt{3}}{2} \cdot \frac{F}{A_v} \tag{1}$$

$$\varphi = \left| \frac{2}{\sqrt{3}} \cdot \ln\left(\frac{t_0}{(t_0 - \Delta t)}\right) \right| - \varepsilon_{el} \tag{2}$$

A_v is the product of the punch width l_p and the actual width of the specimen, t_0 the original thickness of the specimen and Δt the distance traveled by the punch. The plastic strain results from the difference between the total strain and the strain ε_{el} until the yield stress is reached. Since this is a comparative study, plastic flow was assumed for all specimens from an elongation of 0.02%.

Microstructure analysis.

Dynamic image analysis according to ISO 13322-2 using the CAMSIZER X2 particle analyzer from Microtrach Retsch GmbH resulted in percentiles D10 = 20 µm, D50 = 32 µm and D90 = 46 µm. The chemical composition of the powder was determined using the BRUKER TIGER S8 fluorescence spectrometer from Bruker Corporation.

To evaluate the microstructure, the specimens were cut perpendicular to the axis of motion of the punches and embedded in an electrically conductive resin. The specimens were then surface ground with 240-1200 µm grit sandpaper, polished with a diamond suspension, and final polished with a < 0.05 µm silica solution. Samples were etched for 12 s and at a temperature of 60°C in V2A acid solution (100 ml water, 100 ml hydrochloric acid and 10 ml nitric acid) and subsequently analyzed using Thermo Fisher Scientific Inc.'s Phenom XL Generation 2 desktop SEM. Both BSD detector analysis and EDX analysis were performed. For EDX analysis, three areas were examined in each sample, from which the mean value was determined.

Results and Discussion

Chemical composition.

Since the very high temperature of over 2800°C [26] for a short time can lead to the evaporation of individual elements and thus influence the mechanical properties, an EDX analysis was performed on all samples over an area of approximately 0.2 mm² (Table 1). From the measurements it can be seen that some of the main elements are lost during the LPBF process and therefore the proportion of minor elements increases from 0.1% to up to 2.7 %. In correlation with Fuerschbach et al., this burnup occurs particularly for the elements iron and nickel, with the manganese content also decreasing slightly [27]. In contrast, the molybdenum content increases by approx. 1 wt.% and the silicon content by 0.1 wt.%. The measured values are in a similar range for all samples regardless of the orientation and the manufactured geometry, so that it can be assumed that the determined flow curves do not vary decisively due to the chemical composition.

Materials Research Proceedings 28 (2023) 149-158 https://doi.org/10.21741/9781644902479-17

Table 1. Chemical composition [wt.%] of the used 316L powder.

Alloy element	**Fe**	**Cr**	**Ni**	**Mo**	**Mn**	**Si**	**other**
Powder	67.7	17.5	11.3	1.6	1.2	0.6	0.1
Block 1 0° 3 mm	65.9	17.3	10.4	2.6	0.9	0.7	2.2
Block 1 0° 1.5 mm	66.3	17.5	10.7	2.5	1.0	0.8	1.2
Block 4 90° 3 mm	66.0	17.3	10.3	2.6	0.9	0.7	2.2
Block 4 90° 1.5 mm	65.4	17.2	10.5	2.7	0.9	0.7	2.6
Wall 0° 3 mm	66.3	17.4	10.5	2.7	0.9	0.7	1.5
Wall 0° 1.5 mm	65.9	17.5	10.8	2.5	1.0	0.7	1.6
Wall 90° 3 mm	65.7	17.4	10.4	2.6	0.9	0.7	2.3
Wall 90° 1.5 mm	65.5	17.3	10.2	2.6	1.0	0.7	2.7

Microstructure analysis.

Fig. 3 a) shows the microstructure of the specimens prepared in different orientations and initial geometries. To compare the grain sizes, three large grains were marked in each image. It can be seen that the grains in the samples eroded from the blocks are larger than those of the walls. The line intersection method was used to determine the average grain size, which was 27.0 µm for "Block 1 0°," 19.5 µm for "Block 4 90°," and 18.5 µm for "Wall 0°." Due to insufficient etching, the average grain size of "Wall 90°" could not be determined. A smaller grain size leads to an increased yield strength and improved ductility as a result of grain refinement strengthening [28].

Furthermore, it can be seen in Fig. 3 a) that the microstructure and grains of specimens fabricated in 0° orientation are stretched in the build direction and perpendicular to the compression direction, respectively. This results in anisotropy, with specimens fabricated in 0° orientation having lower tensile strength than those fabricated in 90° orientation [29]. Relative to the same specimen cross-section, the specimens printed in 90° orientation exhibit a more spherical grain structure regarding the x-y-plane. The direction of grain growth is influenced by the heat flux, which flows through the component to a large extent in the opposite direction of construction [30]. Therefore, the grains of the components produced by the LPBF method exhibit elongation in the build direction (Fig. 3 b)).

In all fabricated specimens, a cellular substructure is formed, with the dark core elements demarcated by light edge regions (Fig. 4). According to Prashanth et al. and Zhong et al., this substructure is formed by a local enrichment of heavy elements, such as molybdenum, due to a high solidification rate and associated effects of constitutional undercooling [31, 32]. In addition, the shell areas of the cells have a high dislocation density and thus increase the mechanical properties of the printed samples [33]. Due to the layered structure, the cells pass through several heating phases, which reduces the solidification rate, especially in areas far from the surface [30]. Therefore, larger cells are found on the surface.

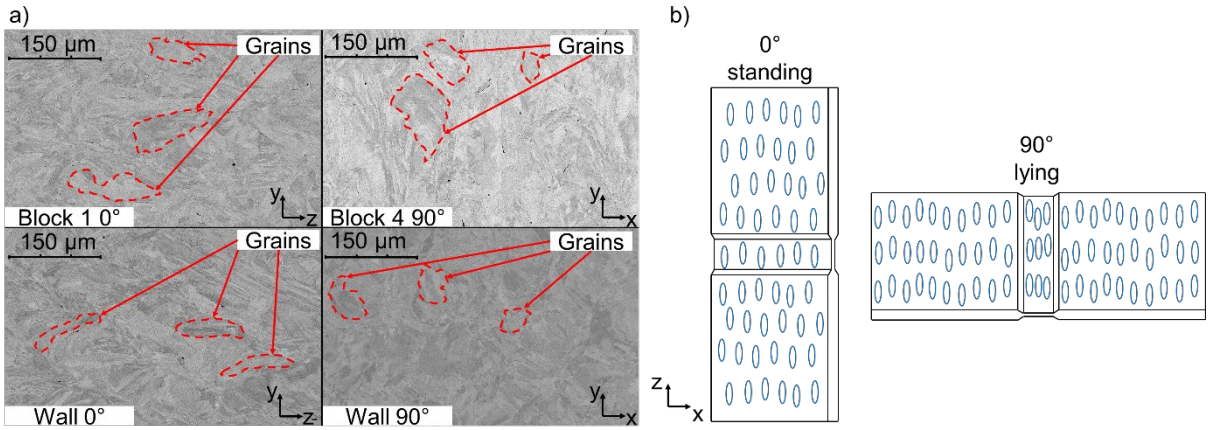

Fig. 3. Detected texture and grain sizes within SEM investigation of the a) Block 1 0°, Block 4 90°, wall 0° and 90° at a thickness of 3mm and b) stretching of the grains depending on the orientation of the printed samples.

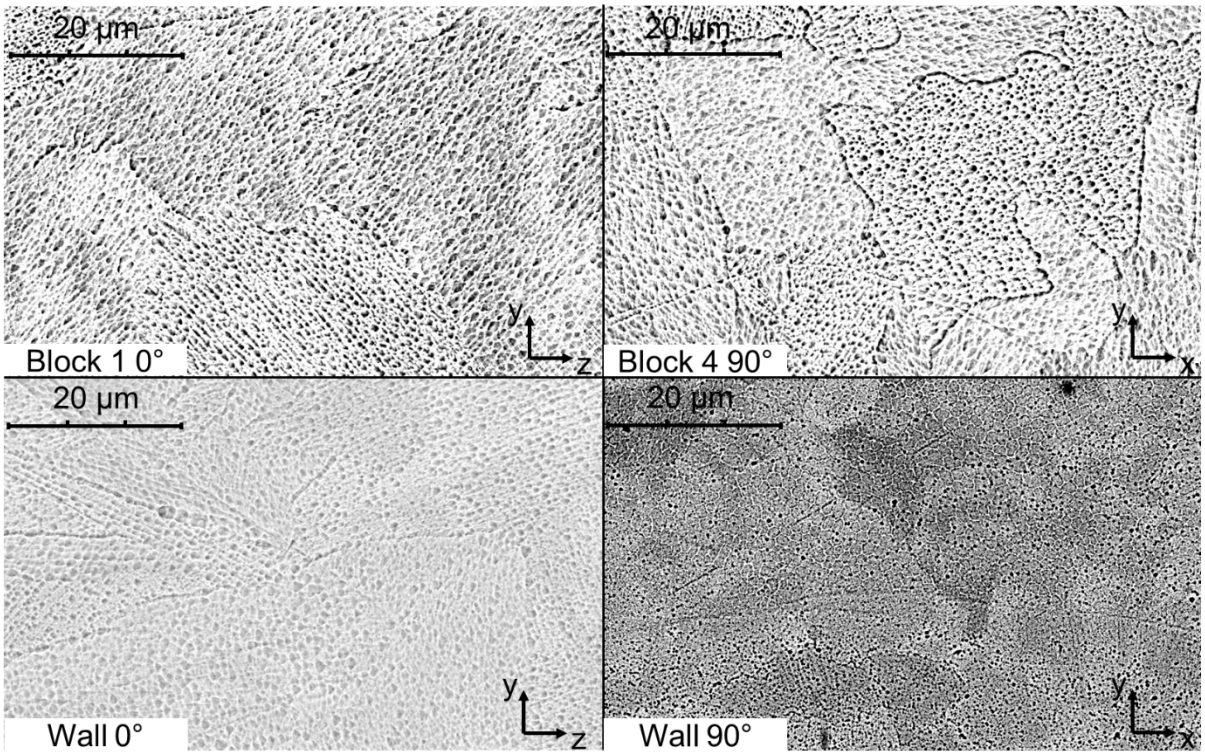

Fig. 4. Cellular substructure within SEM investigation of the a) Block 1 0°, b) Block 4 90°, c) wall 0° and d) wall 90° at a thickness of 3 mm.

Flow curves.

Finally, the qualitative difference in mechanical properties between thin and thick LPBF-manufactured specimens is shown. For this purpose, the repeatability of the compression tests is first presented using three flat compression specimens of equal thicknesses each made from three blocks in 0° orientation (Fig. 5 a)) and 90° orientation (Fig. 5 b)). In the figure, the influence of friction and shear due to the different ratio of punch width (constant) and specimen thickness (1.0, 1.5, 2, 3 mm) can be seen. The scatter increases with decreasing specimen thickness, so that the result for 1.0 mm is not included in the evaluation.

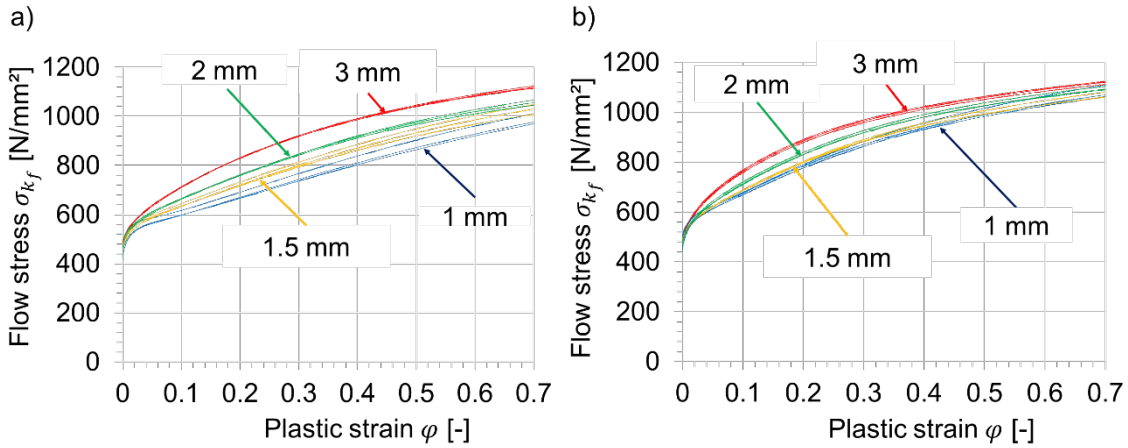

Fig. 5. Flow curves for specimens of thicknesses 1 mm, 1.5 mm, 2 mm and 3 mm taken respectively from blocks printed in a) 0° orientation and b) 90° orientation.

Fig. 6 shows the results for the directly printed walls, where the orientation again gives a clear difference in strength. However, as with the samples from the blocks, the same clear trend can be seen. In order to be able to make qualitative statements regarding the strength change due to the material properties exclusively on the basis of tests, the same specimen thickness from the block is compared with the printed specimen in the following.

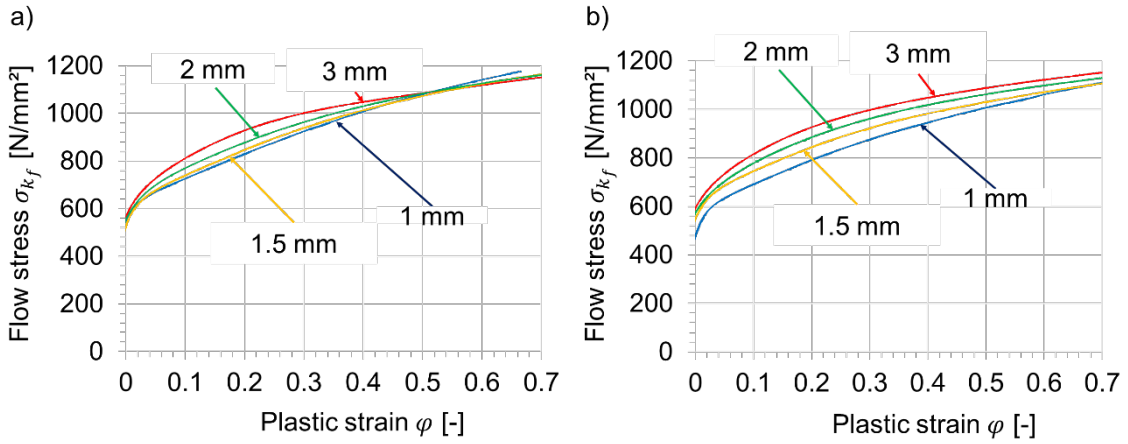

Fig. 6: Flow curves for as-printed plane-strain-compression-specimens at an orientation of the blocks of a) 0° and b) 90°.

Fig. 7 shows the flow curves for specimens with a thickness of 1.5 mm (a)) and 3 mm (b)) up to a plastic strain of 0.7. Both specimen thicknesses show higher flow stresses of the printed walls than the specimens of the same thickness from the blocks. The qualitative progression of the flow curves shows small differences, which are, however, not related to the material condition, but are rather seen in the test setup, or the specimen preparation.

The specimen printed in 0° orientation (block, 1mm) shows a lower slope than the specimen printed in 90° orientation up to a corrected plastic strain of approx. 0.25. From this value, the curves converge again up to the corrected equivalent plastic strain of 0.7. In contrast, the 1mm thick walls diverge from a plastic deformation of 0.2. It should be mentioned again that the grain growth of the specimen printed in 0° orientation was perpendicular to the punch width b_p and in 90° orientation parallel to the punch width b_p (Fig. 3 b)).

In the flow curves determined in the plane-strain-compression-test, this behaviour agrees only for the 1.5 mm thick walls. The flow curves of the 3 mm thick specimens from the block initially

show minor differences and finally meet at a yield stress of approx. 1110 N/mm². Thus, the analysis of the yield stress as a function of the compression direction or orientation in the build space leads to the result that no clear correlation can be identified. This result is confirmed in particular by the 3 mm thick walls.

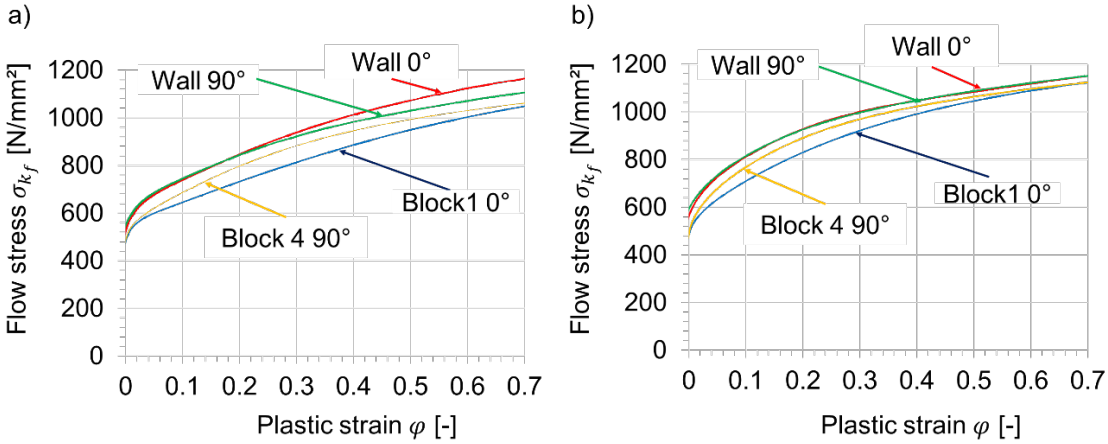

Fig. 7. Calculated flow curves for plane-strain-compression-specimens with a thickness of a) 1.5 mm and b) 3 mm.

Summary

In this work, the mechanical properties of different specimen geometries produced by the LPBF method were investigated in the plane strain compression test. The work shows that different mechanical properties can occur in components depending on the geometry. This results in a locally varying property profile for geometries with high complexity, which are usually produced by the LPBF method. Based on the research, the following conclusions can be drawn:

- The chemical composition of different LPBF specimen geometries is not significantly different.
- The grains are elongated along the build direction (for a specimen orientation of 0° perpendicular to the punch width and for a specimen orientation of 90° parallel to the punch width) and are larger for thick structures than for thin structures.
- The flow stress is significantly dependent on the component thickness and the orientation in the build space. The thinner the sample is printed, the higher the yield stress becomes compared to strips of the same thickness made from blocks. The influence of the orientation in the build space could not be clearly correlated.
- In areas close to the surface, a more pronounced cellular substructure develops due to a higher solidification rate, which also positively influences the mechanical performance.
- The plane-strain-compression-test is an effective test method to quickly obtain flow curves even from thin additive manufactured specimens. Thus, it is possible to estimate the effects of the local microstructure on the flow curve.

An industrial application is the consideration of these manufacturing-specific properties in the topology and structure optimization of components. However, further investigations are necessary for the practical application of the results in optimization programs. Accordingly, further geometries are to be considered in future investigations. In addition, a more detailed investigation of the phase composition and the resulting mechanical properties as a function of the manufacturing geometry is necessary.

References

[1] M. Graf, S. Fritsch, B. Awiszus, Determination of Forming Behaviour of EN AW-6060 by Different Testing Methods under Cold Bulk Forming Conditions, Procedia Manuf. 47 (2020) 1512-1519. https://doi.org/10.1016/j.promfg.2020.04.339

[2] M. Korpela, N. Riikonen, H. Piili, A. Salminen, O. Nyrhilä, Additive Manufacturing - Past, Present, and the Future, In: Collan, M., Michelsen, KE. (eds) Technical, Economic and Societal Effects of Manufacturing 4.0. Palgrave Macmillan, Cham., 2020, pp 17-41 https://doi.org/10.1007/978-3-030-46103-4_2
[3] J. Liu, A.T. Gaynor, S. Chen, Z. Kang, K. Suresh, A. Takezawa, L. Li, J. Kato, J. Tang, C.C.L. Wang, L Cheng, X. Liang, A.C. To, Current and future trends in topology optimization for additive manufacturing, Structural and Multidisciplinary Optimization 57 (2018) 2457-2483. https://doi.org/10.1007/s00158-018-1994-3
[4] H. Monteiro, G. Carmona-Aparicio, I. Lei, M. Despeisse, Energy and material efficiency strategies enabled by metal additive manufacturing - A review for the aeronautic and aerospace sectors, Energy Reports 8 (2021) 298-305. https://doi.org/10.1016/j.egyr.2022.01.035
[5] C. Van Sice, J. Faludi, Comparing Environmental Impacts of Metal Additive Manufacturing to Conventional Manufacturing, International Conference on Engineering Design, Proceedings of the Design Society 1 (2021) 671-680. https://doi.org/10.1017/pds.2021.67
[6] J. Holoch, S. Lenhardt, S. Revfi, A. Albers, Design of Selective Laser Melting (SLM) Structures: Consideration of Different Material Properties in Multiple Surface Layers Resulting from the Manufacturing in a Topology Optimization, Algorithms 15 (2022) 99. https://doi.org/10.3390/a15030099
[7] B. Brown, W. Everhart, J. Dinardo, Characterization of bulk to thin wall mechanical response transition in powder bed AM, Rapid Prototyping Journal 22 (2016) 801-809. https://doi.org/10.1108/RPJ-10-2015-0146
[8] S. Astafurov, E. Astafurova, Phase Composition of Austenitic Stainless Steels in Additive Manufacturing: A Review, Metals 11 (2021) 1052. https://doi.org/10.3390/met11071052
[9] J. Zhu, H. Zhou, C. Wang, L. Zhou, S. Yuan, W. Zhang, A review of topology optimization for additive manufacturing: Status and challanges, Chinese Journal of Aeronautics 34 (2021) 91-110. https://doi.org/10.1016/j.cja.2020.09.020
[10] M. Ragavendran, M. Vasudevan, Laser and hybrid laser welding of type 316L(N) austenitic stainless steel plates, Mater. Manuf. Process. 35 (2020) 922-934. https://doi.org/10.1080/10426914.2020.1745231
[11] M. Ma, Z. Wang, X. Zeng, A comparison on metallurgical behaviors of 316L stainless steel by selective laser melting and laser cladding deposition, Mater. Sci. Eng. A 685 (2017) 265-273. https://doi.org/10.1016/j.msea.2016.12.112
[12] T. Maity, N. Chawake, J. T. Kim, J. Eckert, K. G. Prashanth, Anisotropy in local microstructure - Does it affect the tensile properties of the SLM samples?, Manuf. Lett. 15 (2018) 33-37. https://doi.org/10.1016/j.mfglet.2018.02.012
[13] Q. Zhang, J. Xie, Z. Gao, T. London, D. Griffiths, V. Oancea, A metallurgical phase transformation framework applied to SLM additive manufacturing processes, Mater. Design 166 (2019) 107618. https://doi.org/10.1016/j.matdes.2019.107618
[14] J. Nitzler, C. Meier, K. W. Müller, W. A. Wall, N. E. Hodge, A novel physics-based and data supported microstructure model for part-scale simulation of laser powder bed fusion of Ti-6Al-4V, Advance Modelling and Simulation in Engineering Sciences 8 (2021) 16. https://doi.org/10.1186/s40323-021-00201-9
[15] P. Zhang, J. Liu, A. C. To, Role of anisotropic properties on topology optimization of additive manufactured load bearing structures, Scripta Mater. 135 (2017) 148-152. https://doi.org/10.1016/j.scriptamat.2016.10.021
[16] W. Wang, D. Munro, C. C. L. Wang, F. van Keulen, J. Wu, Space-time topology optimization for additive manufacturing, Struct. Multidisc. Optim. 61 (2020) 1-18. https://doi.org/10.1007/s00158-019-02420-6

[17] A. Nádai, „Plasticity: A Mechanics of the Plastic State of Matter, Nature 131 (1933). https://doi.org/10.1038/131383c0
[18] E. Orowan, The Calculation of Roll Pressure in Hot and Cold Flat Rolling, Procee. of the Insti. of Mech. Eng. 150(1) (1943) 140-167. doi:10.1243/PIME_PROC_1943_150_025_02
[19] A. B. Watts, H. Ford, An experimental investigation of the yielding of strip between smooth dies, Procee. of the Insti. of Mech. Eng. 167(1b) (1953) 448-464. doi:10.1177/002034835316701b28
[20] C. M. Sellars, G. J. Davies, Hot Working and Forming Processes, Proceedings of an International Conference on Hot Working and Forming Processes, Metals Soc., 1980.
[21] N. Becker, Weiterentwicklung von Verfahren zur Aufnahme von Fließkurven im Bereich hoher Umformgrade, Springer Berlin, Heidelberg, Stuttgart, 1994. https://doi.org/10.1007/978-3-662-10890-1
[22] P. Frey, Umformtechnische Strukturierung metallischer Einleger im Folgeverbund für mediendichte Kunststoff-Metall-Hybridbauteile, PhD Thesis, Friedrich-Alexander-Universität Erlangen-Nürnberg (FAU), 2021.
[23] N. Becker, K. Pöhlandt, K. Lange, Improvement of the Plane-Strain Compression Test for Determining Flow Curves, CIRP Annals 38(1) (1989) 227-230. https://doi.org/10.1016/S0007-8506(07)62691-2
[24] M.S. Mohebbi, A. Akbarzadeh, Y.-O. Yoon, S.-K. Kim, Flow stress analysis of ultrafine grained AA 1050 by plane strain compression test, Mater. Sci. Eng. A 593 (2014) 136-144. https://doi.org/10.1016/j.msea.2013.11.027
[25] A.P. Carvalho, L.M. Reis, R.P. Pinheiro, P.H.R. Pereira, T.G. Langdon,
R.B. Figueiredo, Using Plane Strain Compression Test to Evaluate the Mechanical Behavior of Magnesium Processed by HPT, Metals 12 (2022) 125. https://doi.org/10.3390/met12010125
[26] F. Yan, W. Xiong, E. Faierson, G.B. Olson, Characterization of nano-scale oxides in austenitic stainless steel processed by powder bed fusion, Scripta Mater. 155 (2018) 104-108. https://doi.org/10.1016/j.scriptamat.2018.06.011
[27] P.W. Fuerschbach, J.T. Norris, X. He, T. DebRoy, Understanding Metal Vaporization from Laser Welding, Sandia National Laboratories, Albuquerque, 2003.
[28] B. AlMangour, D. Grzesiak, J.-M. Yang, Rapid fabrication of bulk-form TiB2/316L stainless steel nanocomposites with novel reinforcement architecture and improved performance by selective laser melting, J. Alloy. Compd 680 (2016) 480-493. https://doi.org/10.1016/j.jallcom.2016.04.156
[29] A. Fedorenko, B. Fedulov, Y. Kuzminova, S. Evlashin, O. Staroverov, M. Tretyakov, E. Lomakin, I. Akhatov, Anisotropy of Mechanical Properties and Residual Stress in Additively Manufactured 316L Specimens, Materials 14 (2021) 7176. https://doi.org/10.3390/ma14237176
[30] A. Röttger, J. Boes, W. Theisen, M. Thiele, C. Esen, A. Edelmann, R. Hellmann, Microstructure and mechanical properties of 316L austenitic stainless steel produced by different SLM devices, Int. J. Adv. Manuf. Technol. 108 (2020) 769-783. https://doi.org/10.1007/s00170-020-05371-1
[31] K. Prashanth, J. Eckert, Formation of metastable cellular microstructures in selective laser melted alloys, J. Alloy. Compd. 707 (2017) 27-34. https://doi.org/10.1016/j.jallcom.2016.12.209
[32] Y. Zhong, L. Liu, S. Wikman, D. Cui, Z. Shen, Intergranular cellular segregation network structure strengthening 316L stainless steel prepared by selective laser melting, J. Nuc. Mater. 470 (2016) 170-178. https://doi.org/10.1016/j.jnucmat.2015.12.034
[33] A.J. Birnbaum, J.C. Steuben, E.J. Barrick, A.P. Iliopoulos, J.G. Michopoulos, Intrinsic strain aging, Σ3 boundaries, and origins of cellular substructure in additively manufactured 316L, Additive Manuf. 29 (2019) 100784. https://doi.org/10.1016/j.addma.2019.100784